Received: 10 May 2021 | Revised: 28 April 2022 | Accepted: 2 May 2022

DOI: 10.1002/eqe.3665

WILEY

RESEARCH ARTICLE

Structure–soil–structure interaction (SSSI) of adjacent buildings with shallow foundations on liquefiable soil

Konstantinos Kassas[1] | **Orestis Adamidis**[2] | **Ioannis Anastasopoulos**[1]

[1]Institute of Geotechnical Engineering (IGT), Swiss Federal Institute of Technology (ETH), Zürich, Switzerland

[2]Department of Engineering Science, University of Oxford, Oxford, UK

Correspondence
Ioannis Anastasopoulos, Institute of Geotechnical Engineering (IGT), Swiss Federal Institute of Technology (ETH), Zürich, Switzerland.
Email: ixa@ethz.ch

Abstract

This paper studies the effect of structure–soil–structure interaction (SSSI) on the seismic response of neighboring structures with shallow foundations on liquefiable sand. The problem is studied through coupled hydromechanical analyses. Nonlinear soil response is modeled with PM4Sand, calibrated on the basis of soil element tests of Hostun sand. The numerical methodology has been compared against six centrifuge model tests, showcasing its ability to predict the settlements. Three idealized structures of width B are considered, of different aspect ratio and foundation bearing pressure q, founded on two liquefiable layer depths, $D_L/B = 1$ and 2. Initially, the response of a single building is studied, offering insights on the developing failure mechanisms. While the settlement increases with q in the case of a deep ($D_L/B = 2$) layer, this is not the case for the shallow ($D_L/B = 1$) layer, where the increased soil confinement leads to the development of a stiffer soil column, which offers increased support to the structure. Pairs of identical structures are subsequently analysed, revealing the effect of SSSI on settlement (w) and rotation (ϑ). While its effect on w is beneficial, its effect on ϑ is detrimental, leading to a dramatic increase compared to the single structure. The detrimental effect of SSSI on ϑ is shown to be a function of the gap (s/B) between the buildings and the depth of the liquefiable layer (D_L/B). In the case of the shallow layer, the two structures rotate away from each other. This is not the case of the deeper layer, where they may either rotate away or towards each other, depending on s/B.

KEYWORDS

deformation mechanism, liquefaction, numerical modeling, PM4Sand, shallow foundations, structure–soil–structure interaction

1 | INTRODUCTION

Earthquake-induced soil liquefaction is one of the most devastating natural hazards. Despite advancements in seismic codes, structures founded on shallow foundations resting on saturated sandy soil have repeatedly been reported to experience excessive settlement, rotation,[1,2] or even complete toppling[3] as a result of liquefaction during major seismic events. In

recent years, a variety of methodologies have been developed and employed in liquefaction research, offering significant progress in particular on the response of structures founded on shallow foundations.

Several researchers have analyzed well-documented case histories after major earthquakes, offering valuable evidence on the effects of soil liquefaction on the response of real structures. Sancio et al.[4] studied several cases from the 1999 Kocaeli earthquake, which led to severe damage or even toppling collapse of a multitude of buildings in Adapazari. It was concluded that taller buildings (with a larger number of storeys) were observed to accumulate larger settlement and rotation. Studying the same case histories, Gazetas et al.[5] concluded that the effect of neighboring buildings can be quite significant, being a key factor leading to accumulation of rotation, eventually resulting to toppling of slender buildings. Analyzing a number of case histories from the 2010 Maule earthquake in Chile, Bertalot et al.[6] proposed an empirical graph expressing foundation settlement as a function of bearing pressure (q) and depth of liquefiable layer (D_L). Foundation settlement was found to increase with bearing pressure, but only up to $q = 80$ kPa, after which any further increase led to a beneficial effect in terms of settlement accumulation.

Despite the significance and the valuable evidence offered by real case histories, the occurrence of a major seismic event is a prerequisite, which is not within our control. Even when such events take place (as in the previously discussed examples), the soil properties and the seismic excitation cannot be known with accuracy. Centrifuge modeling offers a controlled environment, where the soil properties can be known with less uncertainty and the input seismic motion is fully controlled. Compared to large-scale shaking table experiments, centrifuge modeling is not only advantageous in terms of cost, but also offers the ability to correctly reproduce the confining soil stresses to be consistent with those of the prototype, thus avoiding scale effects associated with the stress level. Centrifuge testing of structures on shallow foundations resting on liquefiable soil indicates that the accumulation of settlement is primarily due to the static and dynamic deviatoric stresses induced by the foundation, with the volumetric response due to reconsolidation being of only secondary significance.[7] Adamidis and Madabhushi[8] further demonstrated that the developing deformation mechanisms are a function of the depth of the liquefiable layer and the foundation bearing pressure. Employing centrifuge modeling, Bertalot and Brennan[9] experimentally confirmed their previoulsy discussed empirical conclusion (based on the case histories), showing that the settlement increases with q up to a certain stress level, above which a reduction should be expected.

Numerical modeling allows a more comprehensive investigation of the problem, not limited by the resources and time constraints of centrifuge modeling. Neverthelss, sophisticated numerical nonlinear deformation analyses (NDAs) are required due to the complexity of the problem. Several constitutive models have been developed, aiming to capture the response of liquefiable soil (e.g., Refs. [10–17]). Such models typically contain a large number of parameters, which have to be carefully calibrated against soil elements tests (e.g., Ref. [18]). Before extracting reliable results, validation against centrifuge model tests (or real scale shake table tests) is necessary (e.g., Ref. [19, 20]). Based on such numerical analyses, Karamitros et al.[21] observed that the presence of initial deviatoric static stress induced by the foundation is beneficial, as it prevents the excess pore water pressure ratio (r_u) under the foundation from reaching $r_u \approx 1$, as in the field.

Several researchers have proposed simplified methods for the design of shallow foundations on liquefiable soil. Tokimatsu and Seed[22] and Ishihara and Yoshimine[23] developed such simplified methods for the evaluation of free-field settlement of sand deposits due to earthquake-induced liquefaction, which are often used in practice. Bertalot et al.[6] proposed an upper-bound estimate of foundation settlement in function of bearing pressure and liquefiable layer depth, based on empirical evidence from case histories. Bray and Macedo,[24] proposed a simplified method for settlement prediction, based on numerical analyses of shallow foundations on liquefiable soil. Bullock et al.[25,26] developed a probabilistic method for settlement and rotation prediction, combining numerical analyses and case histories. Lately, Adamidis and Madabhushi (2021)[27] proposed a rotational stiffness attenuation relationship for simplified predictions of maximum and residual foundation rotation, using rotational spring and dashpot models.

So far, research has focused on structures in isolation, ignoring Structure–Soil–Structure Interaction (SSSI), despite the fact that its significance has been documented in many case histories from recent major earthquakes. Due to the increased population density, urban centres are at high risk, with most liquefaction disasters taking place in cities. In most real-life cases, the assumption of a single, isolated foundation is unrealistic and potentially un-conservative. Indeed, the very few centrifuge studies that have examined two adjacent foundations at different distances from each other,[28–32] all conclude that ignoring SSSI is un-conservative. For structures sufficiently close to each other, a trend of increased outwards rotation was observed by Hayden et al.,[29] similarly to the well-documented case history of the Teverler buildings in Adapazari (Bray et al. 2000, Figure 1A). Nevertheless, Ref. [31] indicate that inward rotation of adjacent structures may also occur, while inwards rotation has also been observed in the field, as in the example of Figure 1B from the 2018 Hokkaido Eastern Iburi earthquake in Japan.[2]

Although centrifuge modelling offers valuable insights, it cannot be efficiently used to conduct extensive par ametric studies. The experimental results can be used as benchmark to validate numerical models, which can then be used for to

FIGURE 1 Evidence of SSSI in function of distance in between: (A) buildings at a small distance in Adapazari (Turkey), tilting outwards (Bray et al., 2020); and (B) buildings at a large distance in Sapporo's Kiyota Ward (Japan) tilting inwards (*source*: The Asahi Shimbun)

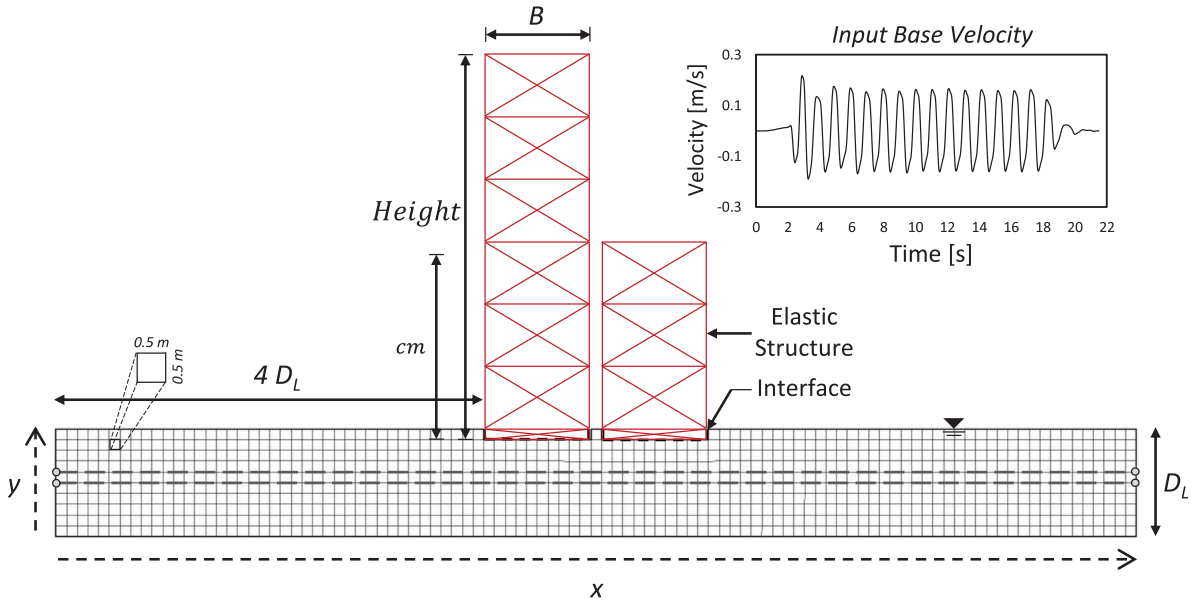

FIGURE 2 Numerical analysis configuration and input motion

parametrically investigate the effects of SSSI on adjacent buildings, which is the key scope of the present paper. Idealised structures of different geometry and foundation bearing pressure are analysed, resting on liquefiable layers of different depth. The plane strain fully-coupled numerical analyses are conducted employing the constitutive model PM4Sand,[11] as implemented in the finite difference (FD) code FLAC 8.1.[33] The constitutive model is calibrated on the basis of soil element tests, conducted at the ETH Zurich (ETHZ) geotechnical laboratory.[18] The numerical methodology employed herein has been compared against six centrifuge model tests of single structures on surface foundations with variable bearing pressures, resting on liquefiable layers of different depths.[19] The first key contribution of the present paper is the in-depth assessment of the effects of SSSI by direct comparison to isolated structures. The second key contribution is the use of the numerical model to investigate the effects of foundation bearing pressure, depth of the liquefiable layer and gap between the structures on the overall mechanisms, the settlement and the rotation of two adjacent buildings.

2 | METHODOLOGY

The problem is analysed assuming plane strain conditions, employing the FD code FLAC 8.1 and the constitutive model PM4Sand (Version 3.1). Nonlinear fully-coupled effective stress time history analyses are conducted, parametrically analysing the response of buildings on raft foundations, with and without neighboring structures. Figure 2 shows an

TABLE 1 Details of the studied building assemblies

Floors	Height H (m)	Aspect ratio h_{cm}/B	Bearing pressure q (kPa)
1	3.5	0.24	22.5
3	9.5	0.79	42.5
6	18.5	1.68	72.5

example of the FD mesh, model geometry, input motion and boundary conditions. Three idealised building types with variable floor number, height (H), and foundation bearing pressure (q) are considered and studied as benchmark cases (Table 1). All the buildings have a width $B = 5$ m and are founded 0.5 m below the ground surface, as was the case for the toppled Teverler buildings in Adapazari (Figure 1A), which largely inspired the present study. Although admittedly narrow, the 5 m width is not only compatible with the Teverler case history (6 m), but also with the University of Cambridge centrifuge model tests that were used for model validation. The total weight of each building consists of the weight of the superstructure, assuming an average load of 10 kN/m^2 per floor and the weight of the foundation slab, taken equal to 12.5 kN/m^2 for all cases examined. To focus on the deformation mechanisms within the soil, the structures are idealized as rigid, being modelled with elastic beam elements of very large stiffness. The mass density of the structural elements is set to match the targeted mass and bearing pressure. The soil-foundation interface is modelled with a frictional interface, allowing for sliding and detachment, while the foundation beam acts as an impermeable barrier.

The lateral model boundaries are positioned at a sufficient distance of four liquefiable layer depths ($4.0D_L$) from the foundation edges to limit boundary effects.[19] A laminar box condition is adopted for the lateral boundaries, where opposite lateral boundary nodes of the same depth are connected. The seismic excitation is the one recorded in one of the centrifuge model tests of Adamidis and Madabhushi,[8] which was used for the assessment of the numerical analysis methodology.[19] The pseudo-harmonic input motion contains 16 cycles with frequency equal to 1 Hz and acceleration amplitude equal to 0.15 g. The corresponding velocity time history (Figure 2) is applied at the bottom of the model, which are fixed in the vertical direction.

Following the recommendations of Boulanger and Ziotopoulou[34], Rayleigh damping is set to 0.5% at a center frequency of 1 Hz, which is the dominant frequency of the input motion. The PostShake Flag parameter of PM4sand is enabled after strong shaking (20 s) to improve the modeling of post-liquefaction reconsolidation. Large deformations and second order effects are taken into account by automatically updating mesh node coordinates after each analysis step.

2.1 | Soil constitutive model

The seismic response of fully saturated Hostun (HN31) sand is simulated using the plane-strain, stress-ratio controlled, critical state compatible, bounding surface plasticity model PM4Sand, Version 3.1.[34] The model has been developed for geotechnical earthquake engineering applications, following the framework of the DM04 model.[13] A detailed description of model formulation and its modifications can be found in Boulanger and Ziotopoulou,[11] Ziotopoulou and Boulanger,[35] and Boulanger and Ziotopoulou.[34]

The model requires a total of 27 input parameters, from which six are considered primary (including the atmospheric pressure and 2 "flag" parameters) and 21 secondary. The primary parameters include the apparent relative density (D_r), the small-strain shear modulus coefficient (G_o), and the contraction rate parameter (h_{po}). Preset values, which are generally functions of an index property, can be used for the secondary parameters, which can also be calibrated against experimental data. To that end, the constitutive model was calibrated here based on the element tests of Hostun (HN31) sand described in detail in Kassas et al.[18], corresponding to a fully saturated layer of Hostun sand with void ratio $e = 0.838$. Table 2 summarizes the calibrated parameters for Hostun (HN31) sand. All the other constitutive model parameters preserve their preset values.

Figure 3A illustrates the cyclic resistance ratio (CRR) versus the load cycles required for liquefaction (N), as estimated by PM4sand for direct simple shear (DSS) element test simulations with initial vertical effective stress $\sigma'_{v0} = 100\ kPa$, based on the aforementioned calibration. The point where shear strain $\gamma = 3.75\%$ in single amplitude (SA) is considered as the criterion for liquefaction triggering. Figure 3B presents the excess pore water pressure ratio (r_u) in function of load cycles, normalised to the required number of load cycles for liquefaction triggering for each case (the dotted line corresponds to $r_u > 0.6$). Roughly after this threshold a rapid drop in effective stress was observed, particularly evident at the stress

TABLE 2 Calibrated soil parameters for Hostun (HN31) sand

Parameter		Value
e (-)	Void ratio	0.838
ρ_d (Mg/m^3)	Dry mass density	1.44
ρ_s (Mg/m^3)	Wet mass density	1.90
e_{min} (-)	Minimum void ratio	0.648
e_{max} (-)	Maximum void ratio	1.049
G_o (-)	Shear modulus coefficient	724.6
h_{p0} (-)	Contraction rate parameter	0.12
φ_{cv} (^{o})	Critical state friction angle	33.8
ν (-)	Poisson ratio	0.308
Q (-)	Bolton's critical state parameter	8.4
R (-)	Bolton's critical state parameter	0.78
k (m/s)	Permeability	9.53E-4

paths of Figure 3D. In all cases examined, the failure line is reached in less than three loading cycles after this threshold, initiating thereafter a rapid shear stiffness degradation (Figure 3C).

2.2 | Comparison against centrifuge model tests

The detailed comparison has been presented in Kassas et al.,[19] where six centrifuge model tests of shallow strip foundations subjected to earthquake-induced liquefaction were simulated using the calibrated PM4Sand constitutive model. Conducted at the Turner Beam Centrifuge of the Schofield Centre at the University of Cambridge, the centrifuge experiments refer to different depths of liquefiable layer and foundation bearing pressures.[8] Figure 4A and B summarize the comparison between computed and measured residual settlement and rotation for all 6 centrifuge model tests. Accumulated settlements were reliably predicted Figure 4A), whereas the simulation efficacy for residual rotations was reduced (Figure 4B). Figure 4C shows the evolution of settlement for a structure with foundation bearing pressure $q = 100\,kPa$ founded on a Hostun (HN31) sand layer of $e = 0.838$ and liquefiable depth $D_L = 2.5B = 11.63\,m$ (prototype scale).

3 | FREE-FIELD RESPONSE

Two soil profiles are analyzed, having liquefiable layer depth $D_L/B = 1$ and 2. Figure 5 compares the free-field response of the two soil profiles in terms of acceleration (a) and excess pore water pressure ratio (r_u) time histories. For each soil profile, the results are presented at three characteristic depths: the base, where the input motion is applied; the middle of the liquefiable soil layer; and the ground surface.

For both layers, a certain point exists when, due to the soil softening close the base of the model, the transmitted acceleration is significantly reduced, the dilation spikes disappear, and r_u is maintained equal to the unit. For this point to be reached, at the middle of the liquefiable layer, 3.98 s of shaking are required for the shallow $D_L/B = 1$ layer (Figure 5A) and 2.59 s for the deeper ($D_L/B = 2$) layer (Figure 5B). This difference is attributed to the lower overburden stress of the shallow layer, which leads to higher cyclic shear resistance (K_σ effect). Before that point, high acceleration spikes are observed, which coincide with dilation-induced drops in r_u. These spikes are more pronounced at the ground surface, where the initial effective stress is minimal.

As expected, faster drainage can also be observed in the case of the shallow layer (Figure 5A), where more pronounced dissipation of excess pore water pressure takes place in the middle of the soil layer, due to the shorter drainage path. Figure 6 depicts the accumulated shear strain contours for $t = 14.34\,s$ with superimposed velocity vectors, for the two examined soil layers. In both cases, a shear zone is observed to develop, with shear strains of the order of 7%. For both D_L/B examined, the shear zone is formed above the mid-depth of the soil layer, being responsible for the previously discussed

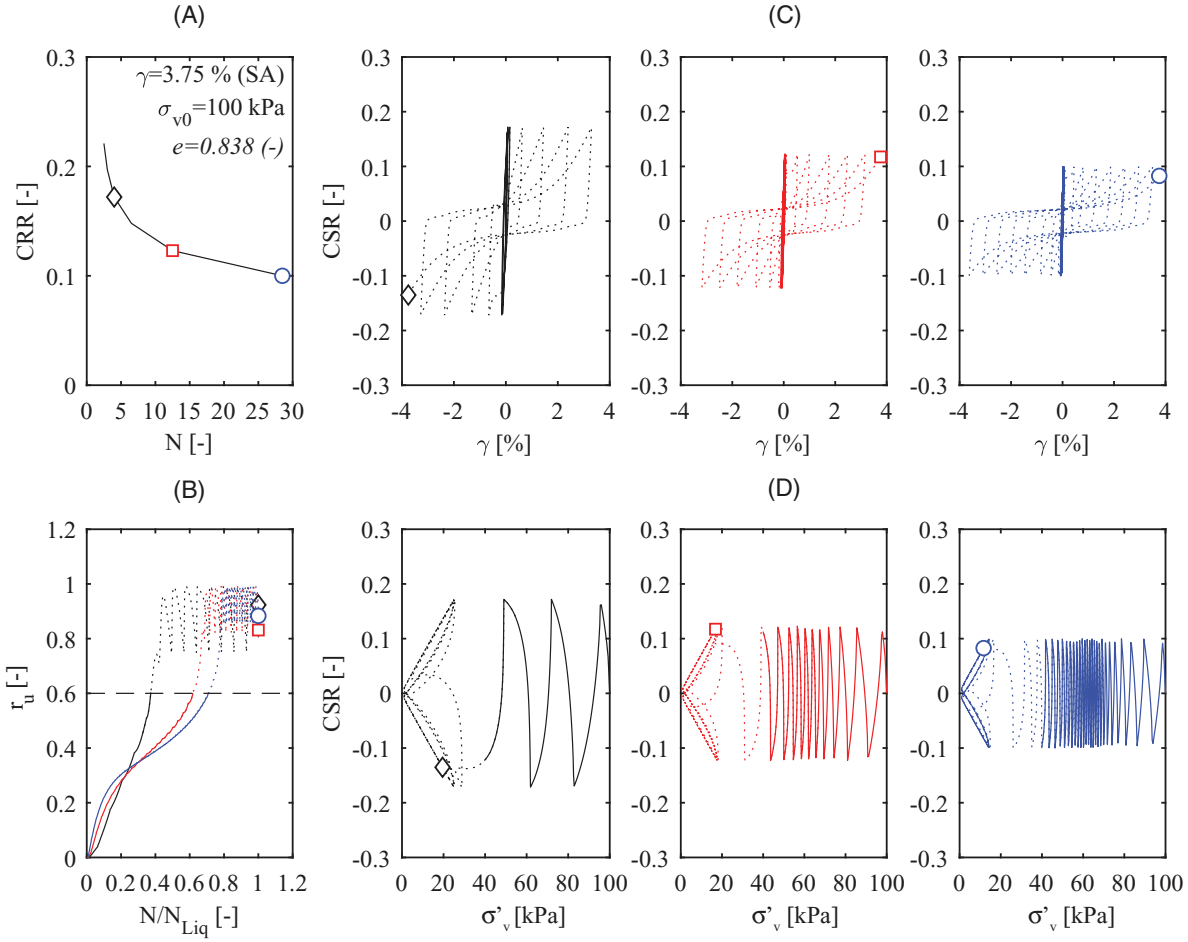

FIGURE 3 Simulation of direct simple shear test of Hostun (HN31) sand using the calibrated PM4Sand model: (A) Cyclic resistance ratio *CRR* in function of load cycles (N), considering liquefaction triggering at $\gamma = 3.75$ % in SA; (B) excess pore water pressure ratio (r_u); (C) shear stiffness degradation; and (D) stress path for *CSR* equal to: 0.172, 0.123 and 0.1

filtering of the transmitted accelerations to the upper half of the soil layer, as imprinted in the ground surface acceleration time histories.

4 | SINGLE BUILDING

A single building is initially studied to gain insights on the key mechanisms affecting the response, and their dependence on bearing pressure (q) and liquefiable layer depth (D_L). The numerical model is identical to the one of Figure 2, with the exclusion of the one building and the corresponding soil elements underneath. As summarized in Table 1, three buildings with q = 22.5, 42.5, and 72.5 kPa (corresponding to 1, 3, and 6 storeys, respectively) are analyzed, founded on liquefiable layers of two different depths: $D_L/\mathrm{B} = 1$ and 2.

Figure 7 compares the settlement–rotation (w–θ) response for the six cases examined. The lightly-loaded ($q = 22.5\,kPa$) structure sustains the smallest settlement for both D_L/B. Its lower bearing pressure, rocking mass, and aspect ratio ($h_{cm}/B = 0.24$) lead to lower normal stresses and rocking moments at the foundation level, limiting both the settlement and the amplitude of rocking oscillations. The moderately-loaded building ($q = 42.5\,kPa$) experiences larger settlement than the lightly-loaded for both D_L/B, which is consistent with the aforementioned reasoning. In both cases ($q = 22.5\,kPa\ and\ 42.5\,kPa$), the settlement increases with liquefiable layer depth D_L/B, in accordance with previous studies.[6,26] Following the same trend, the heavily-loaded ($q = 72.5\,kPa$) building experiences even larger settlement in the case of the deep ($D_L/B = 2$) layer. However, this is not the case for the shallow ($D_L/B = 1$) layer, where despite

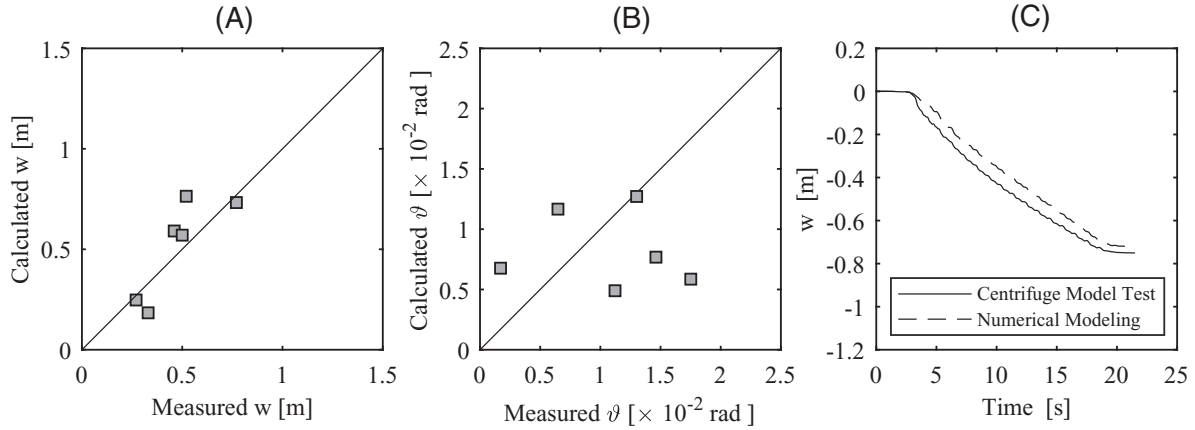

FIGURE 4 Comparison between experimentally measured and predicted: (A) final settlement of six centrifuge test simulations; (B) final rotation of six centrifuge test simulations; and (C) foundation settlement for a centrifuge test with q = 100 kPa and $D_L/B = 2.5$

its increased bearing pressure, rocking mass and aspect ratio, the structure does not accumulate more than half of the settlement of the moderately-loaded structure.

The mechanism driving this behaviour is revealed in Figure 8, which illustrates the computed excess pore-water pressure ratio (r_u) towards the end of the seismic excitation ($t = 17\ s$) for the six studied cases. For both D_L/B, the heavier structure generates a bulb of increased effective stress below the foundation, where r_u does not exceed 0.6, the value after which, pore water pressures increase rapidly (Figure 3B). In the case of the shallow layer (Figure 8A), the increased effective stress bulb reaches the base of the layer, creating a soil column that is much stronger that the surrounding liquefied soil, which offers better support to the structure, thus leading to reduced settlement (Figure 7). In this case, both soil stiffness and bearing capacity increase. On the contrary, in the case of the deep layer (Figure 8B), the heavily-loaded structure sits on this bulb of stronger soil, which is surrounded by the adjacent liquefied soil, but does not reach the base of the layer. Hence, the settlement is not reduced.

Figure 9B illustrates the stress paths at a depth equal to one width below the edge of the foundation (point A) for the heavy structure, for both liquefiable layer depths considered. In both cases, the initial static (due to the bearing pressure acting on the foundation) deviatoric stress is present. However, its effect remains only in the shallow layer (Figure 9A), where it drove the stress path close to the phase transformation and failure lines, leading to more significant dilation, preventing a drastic reduction in effective stress and not allowing stress reversal, which would have led to the accumulation of larger shear strains. In the case of the deep layer (Figure 9B), where the stiffer soil bulb does not reach the base, a rapid redistribution of shear stresses can be observed. This leads to significant reduction of effective stress, resulting in accumulation of large shear strains upon shear stress reversals.

The level of excess pore water pressure ratio in the soil bulb below the foundation and the depth of this bulb is a function of q and D_L/B. As shown in Figure 8, the contribution of the aforementioned change in mechanism is present but not dominant for the medium weight structure. In this case, $r_u > 0.6$ develops below the foundation in the shallow layer (Figure 8A), leading to more intense soil softening (as expected from Figure 3), thus producing large settlement even for the shallow layer (Figure 7). Similarly, in the case of the lightly-loaded structure, the 22.5 kPa of bearing pressure are not enough to create a stiff soil column that reaches the base of the layer in either of the examined depths (Figure 8). Therefore, its beneficial effect on the reduction of settlement cannot materialize (Figure 7). Overall, the weight of the structure appears to have two counteracting effects on settlement. On the one hand, the increased bearing pressure and bending moment acting at the foundation level lead to an increase of the settlement potential. On the other hand, the bulb of increased effective stress under the foundation may reach the base of the liquefiable layer, offering a stiff column of support and leading to the reduction of the settlement potential.

The above conclusions are in line with the experimental observations of Adamidis and Madabhushi[8]. Depending on the thickness of the soil layer, two different deformation mechanisms were identified. In the case of a deep layer, the structure was found to settle primarily due to increased lateral soil displacements, taking place beneath a bulb of stiffer soil formed below the foundation. In more shallow layers, this bulb reached the base of the layer, transmitting large accelerations to the structure and promoting rocking response, with settlement being the result of increased soil displacement under the edges of the foundation.

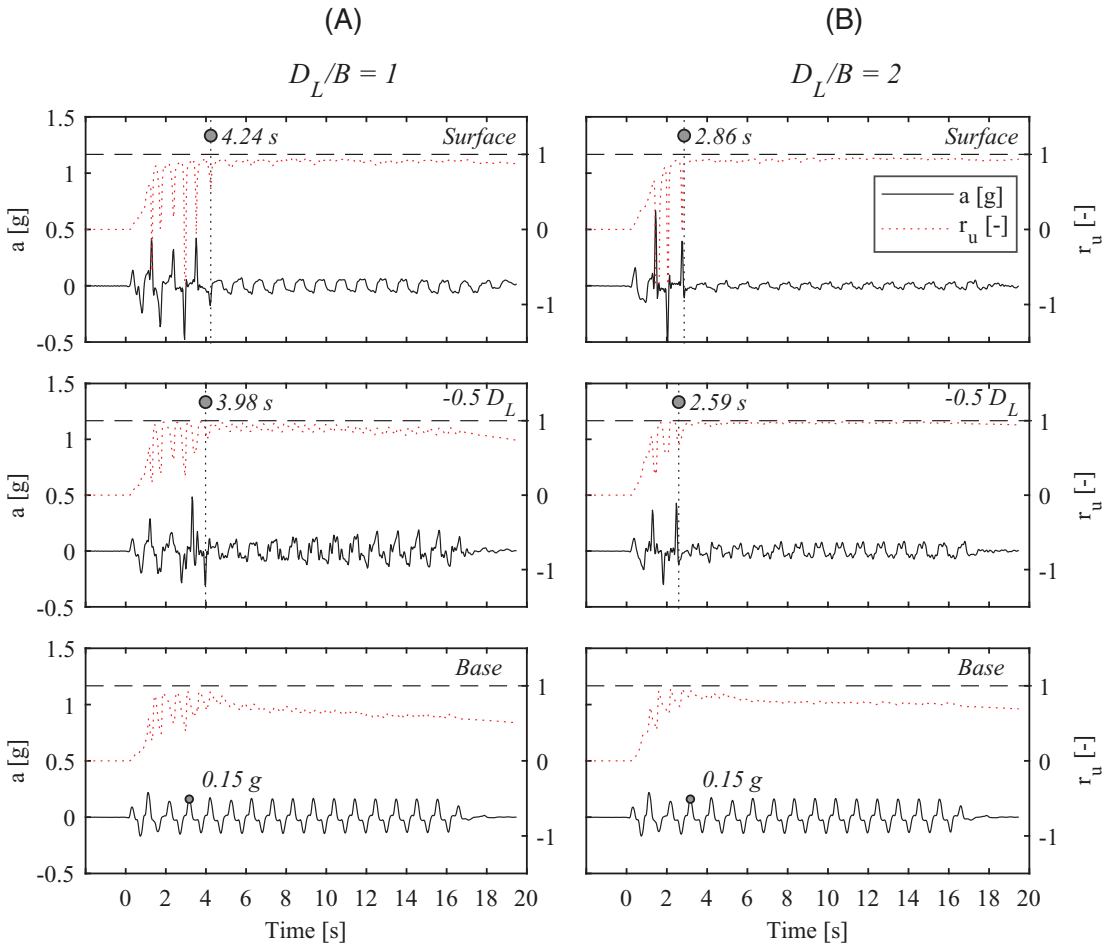

FIGURE 5 Free field response. Time histories of acceleration (a) and excess pore-water pressure ratio (r_u) for two soil layer depths: (A) $D_L/B = 1$; and (B) $D_L/B = 2$

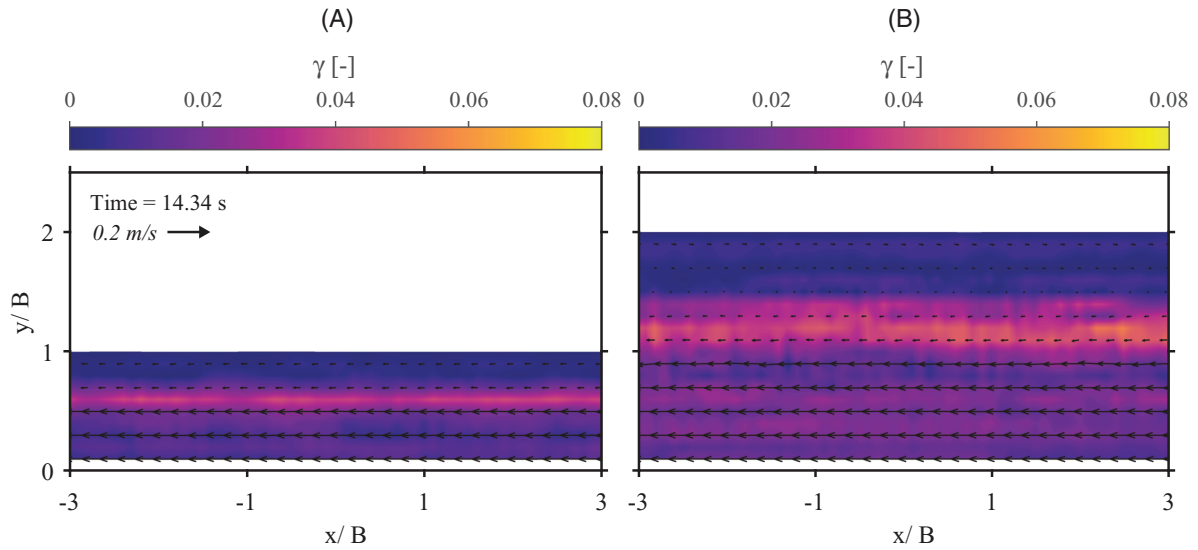

FIGURE 6 Free field response. Contours of accumulated shear strains with superimposed velocity vectors for $t = 14.34$ s, for liquefiable layer depth: (A) $D_L/B = 1$; and (B) $D_L/B = 2$

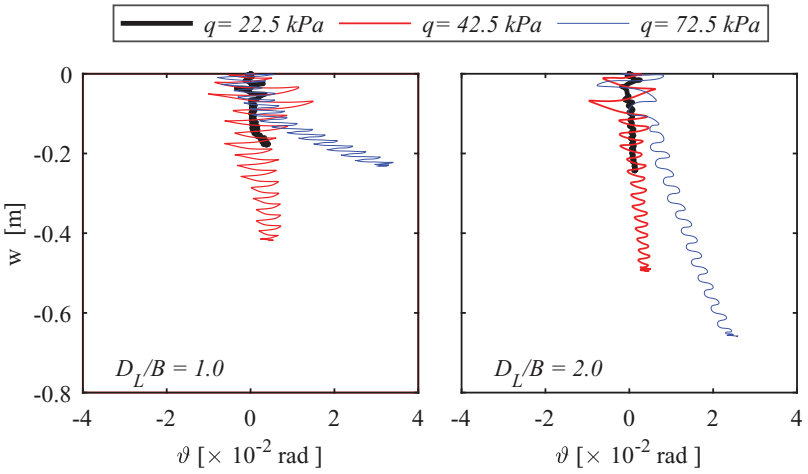

FIGURE 7 Single building settlement–rotation ($w - \vartheta$) response for three different bearing pressures $q = 22.5,\ 42.5,\ and\ 72.5\ kPa$ (corresponding to 1, 3, and 6 storeys, respectively), and two liquefiable layer depths $D_L/B = 1$ (left); and $D_L/B = 2$ (right)

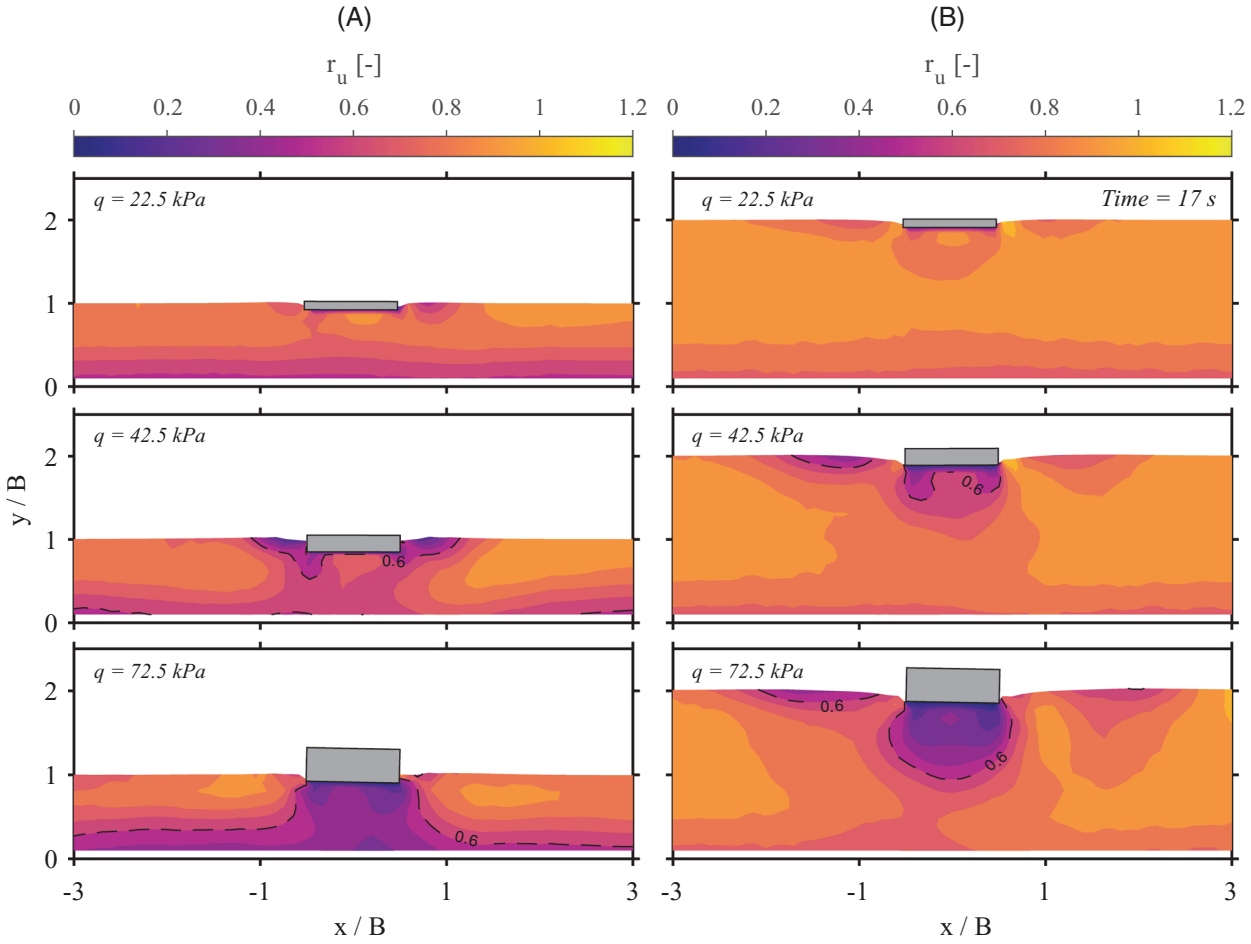

FIGURE 8 Contours of excess pore-water pressure ratio (r_u) at the end of shaking ($t = 17\ s$) for the three bearing pressures examined (top to bottom) and for the two liquefiable layer depths: (A) $D_L/B = 1$; and (B) $D_L/B = 2$

4.1 | Influence of liquefiable layer depth

In this section, the effect of the depth of the liquefiable layer (D_L/B) on settlement is investigated in more detail for the moderately- ($q = 42.5\ kPa$) and the heavily-loaded ($q = 72.5\ kPa$) structures, varying D_L/B from 1 to 2. As shown in Figure 10A, the settlement of the heavily-loaded structure ($q = 72.5\ kPa$) increases with the liquefiable layer depth, up to $D_L/B = 1.8$. Further increase of D_L/B does not lead to any further increase of settlement. With the increase of liquefiable

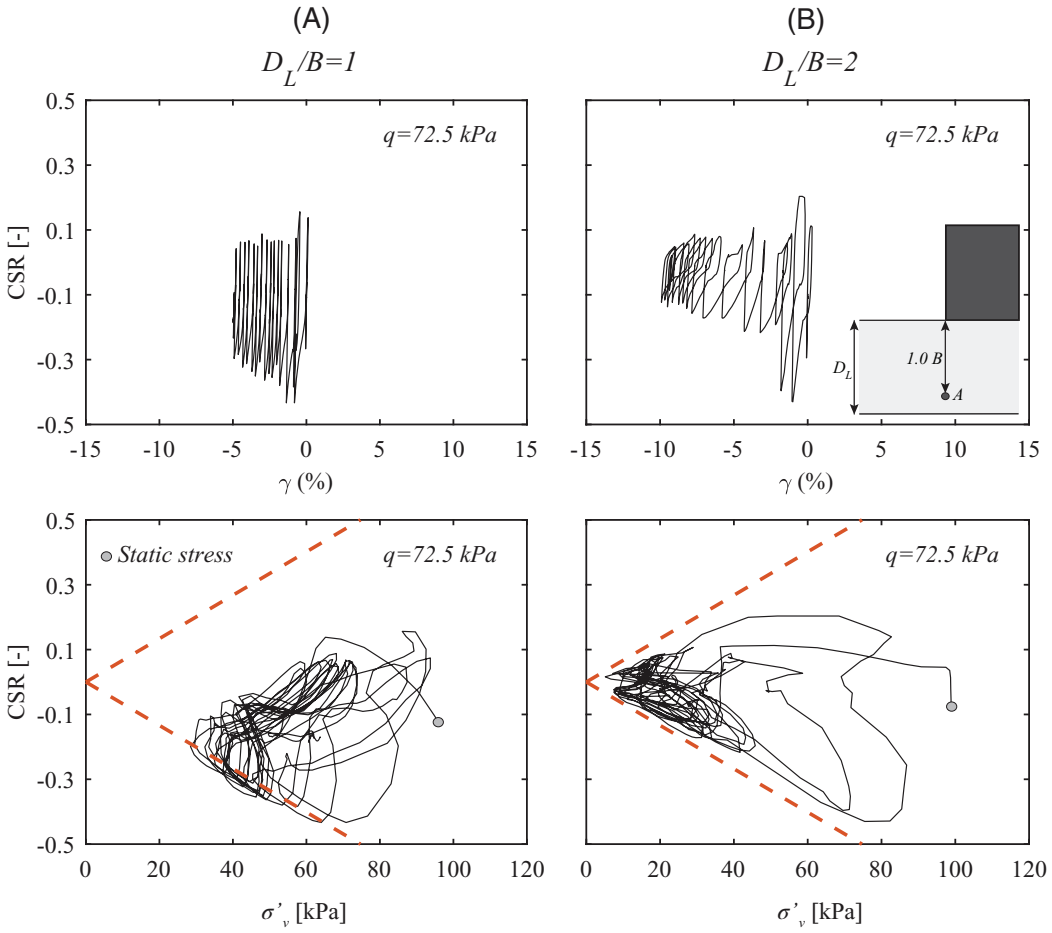

FIGURE 9 Shear stiffness degradation (top) and stress path at a depth $y = B$ below the foundation edge (point A) for the heavily-loaded ($q = 72.5\ kPa$) building, for liquefiable layer depth: (A) $D_L/B = 1$; and (B) $D_L/B = 2$

layer depth, the beneficial effect of the previously discussed column of stiffer soil below the foundation is progressively weakened. As revealed by Figure 10B, the stiffer soil bulb cannot reach the base of the liquefiable layer for $D_L/B \geq 1.4$.

The effect of D_L/B is less significant for the moderately-loaded structure, as the lower bearing pressure ($q = 42.5\ kPa$) is not enough to generate a stiff soil bulb below the foundation, even for a shallow layer of $D_L/B = 1.0$ (Figure 8A). Therefore, the settlement is less sensitive to the liquefiable layer depth. Figure 10A illustrates the boundary between the two aforementioned counteracting mechanisms. Although the heavily-loaded structure imposes larger bearing pressure and rocking moment at the foundation, it sustains less settlement than the moderately-loaded, provided that the forming stiffer soil bulb can reach the base of the liquefiable layer: $D_L/B < 1.4$. For larger depths, the beneficial effect of the supporting stiffer column below the foundation disappears, and the heavily-loaded structure settles more than the moderately-loaded.

The settlement mechanisms described above can be better understood by examining the excess pore water pressure ratio (r_u) below the foundation. Figure 10A plots r_u below the middle of the foundation at a depth $y = 0.2B$ above the base of the model (point A) in function of liquefiable layer depth (D_L/B). The increase of D_L/B leads to an increase of r_u below the structure. Despite the larger shearing imposed to the soil (due to the larger bearing pressure and moment), the developing r_u is lower for the heavily-loaded structure for the entire range of D_L/B. This is attributed to the beneficial effect of vertical loading, which increases the effective stresses below the structure, preventing the pore water pressure ratio from reaching $r_u \approx 1$, as in the free-field. The effect of bearing pressure diminishes with the increase of D_L/B, with the developing r_u becoming almost the same for both structures for $D_L/B = 2$. In addition, as previously discussed, the increased bearing pressure of the heavily-loaded structure also introduces larger static deviatoric stresses below the edges of the foundation, which prevent the reduction of effective stresses there (Figure 9), offering a beneficial effect.

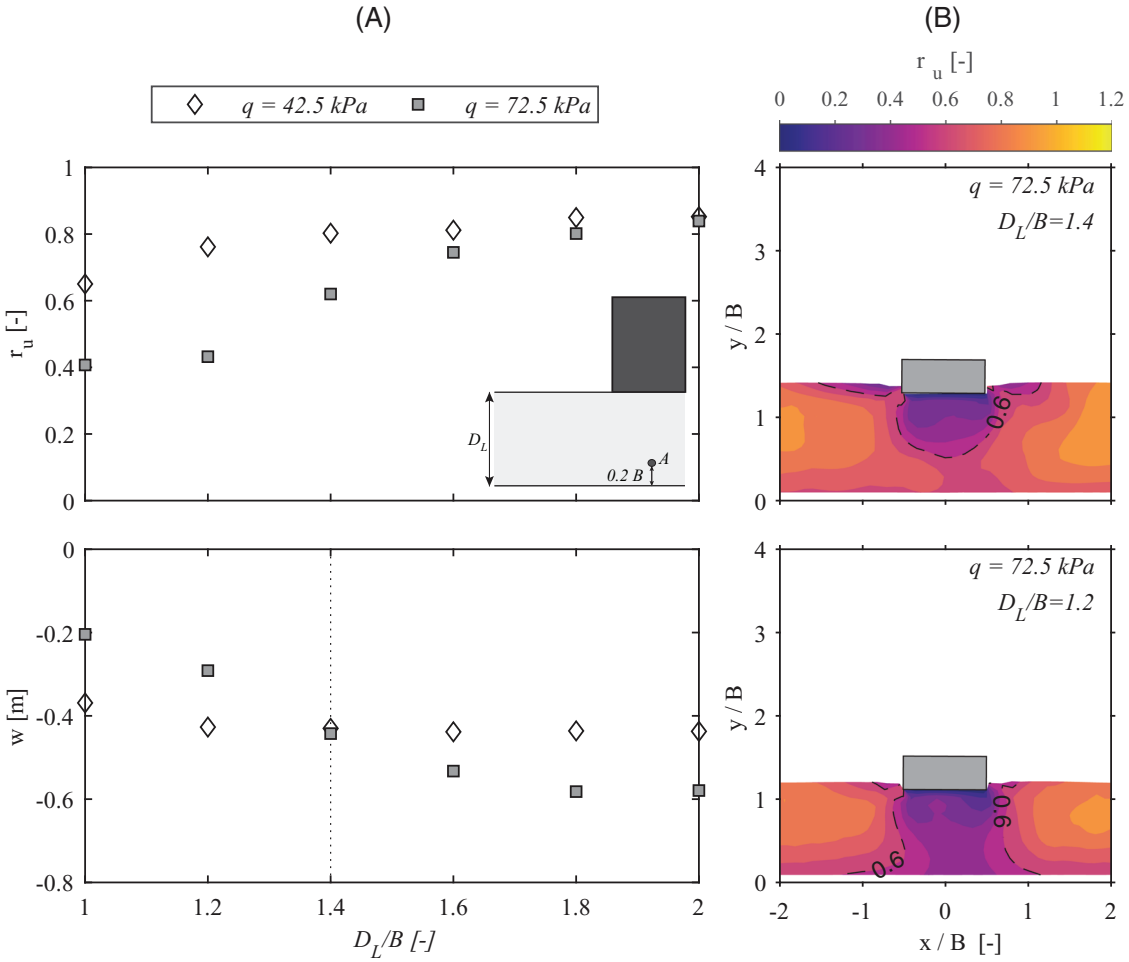

FIGURE 10 Influence of liquefiable layer depth (D_L/B): (A) excess pore water pressure ratio (r_u) at depth $y = 0.2B$ above the midpoint of the model base (point A) and accumulated settlement (w) in function of D_L/B for $q = 42.5\ kPa$ and $72.5\ kPa$; and (B) contours of excess pore-water pressure ratio (r_u) at the end of shaking ($t = 17\ s$) for $q = 72.5\ kPa$ and $D_L/B = 1.4$ (top) and 1.2 (bottom)

4.2 | Failure mechanisms

Figure 11 illustrates the failure mechanisms for the three idealised structures and for the two liquefiable layer depths considered, $D_L/B = 1$ (Figure 11) and $D_L/B = 2$ (Figure 11), in terms of accumulated shear strain contours with superimposed velocity vectors. To allow direct comparisons with free-field response, the results are plotted for the same instant ($t = 14.34\ s$), as in Figure 6.

The mechanisms are easier to identify in the case of the deeper layer (Figure 11). As it would be expected, the presence of the foundation increases significantly the magnitude of accumulated shear strains. In the case of the deep layer, the response bears similarities to that of the free-field. A shear zone is formed at a depth of $0.5D_L$ below the ground surface, above which the transmitted accelerations (and hence velocities) are filtered. Two distinct areas can be distinguished, one below and one above the shear zone. In the area below the shear zone, the soil is moving in phase with the base of the model similarly to the free-field case, but the developing shear strains are larger, due to the static and seismic shear stresses imposed by the foundation. Above the shear zone, the transmitted velocities are filtered and the soil movement is mainly due to mobilisation of foundation bearing capacity. This mechanism becomes more apparent when examining the velocity vectors, and especially for the larger bearing pressure ($q = 72.5\ kPa$), where the increased soil confinement prevents the excessive increase of the pore water pressure ratio r_u (see also Figure 8B), allowing higher accelerations to be propagated to the structure. In the case of the shallow layer (Figure 11), a shear zone is similarly formed at $0.5D_L$ depth below the ground surface, which now overlaps with the mobilised foundation bearing capacity mechanism. Due to the stiffer soil column that forms underneath the foundation, the transmitted accelerations are larger than in the free-field

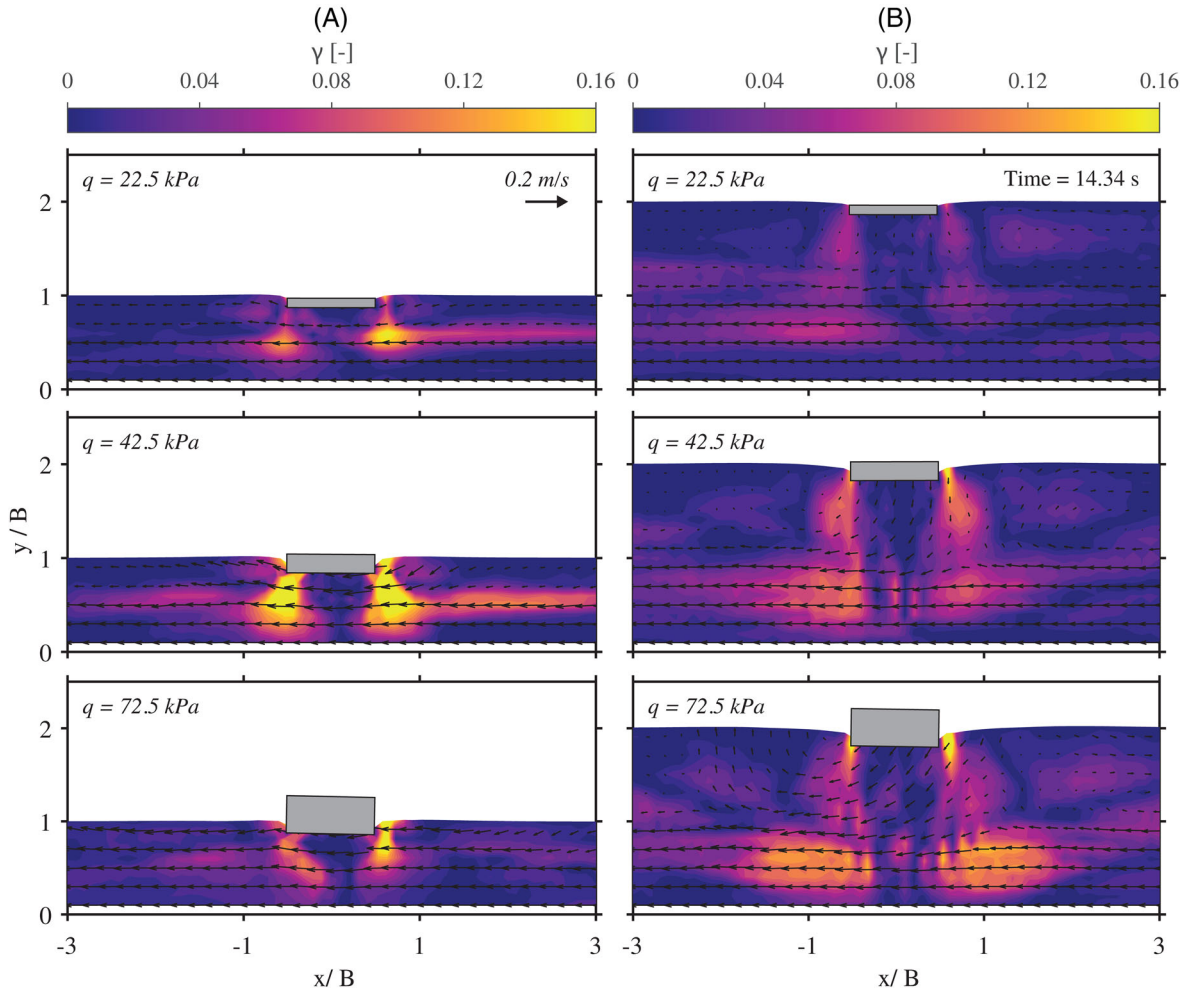

FIGURE 11 Contours of accumulated shear strain with superimposed velocity vectors ($t = 4.34\ s$), for the three structures examined (top to bottom) and for two liquefiable layer depths: (A) $D_L/B = 1$; and (B) $D_L/B = 2$

(Figure 6). This effect becomes more pronounced with the increase of foundation bearing pressure, as indicated by the velocity vectors.

5 | STRUCTURE–SOIL–STRUCTURE INTERACTION (SSSI)

In the absence of soil liquefaction, Structure–Soil–Structure Interaction (SSSI) has been found to be potentially detrimental or beneficial.[36–39] Its effect in the case of liquefiable layers has not been studied to a similar extent. Having identified the critical mechanisms that affect the performance of a single, isolated structure, the effect of neighboring structures is examined. A parametric analysis is conducted, studying the previously discussed configurations of neighboring structures. Exactly the same buildings are analyzed, but now places in pairs. For every pair, two identical structures are examined, with the same aspect ratio and bearing pressure, varying the gap in between. As previously, two liquefiable layer depths are examined, $D_L/B = 1$ and 2.

5.1 | Settlement

Figure 12 illustrates the influence of SSSI on accumulated settlement (i.e., at the end of shaking). The results are presented for the three pairs of structures (lightly-, moderately-, and heavily-loaded) and for the two liquefiable layer depths ($D_L/B =$

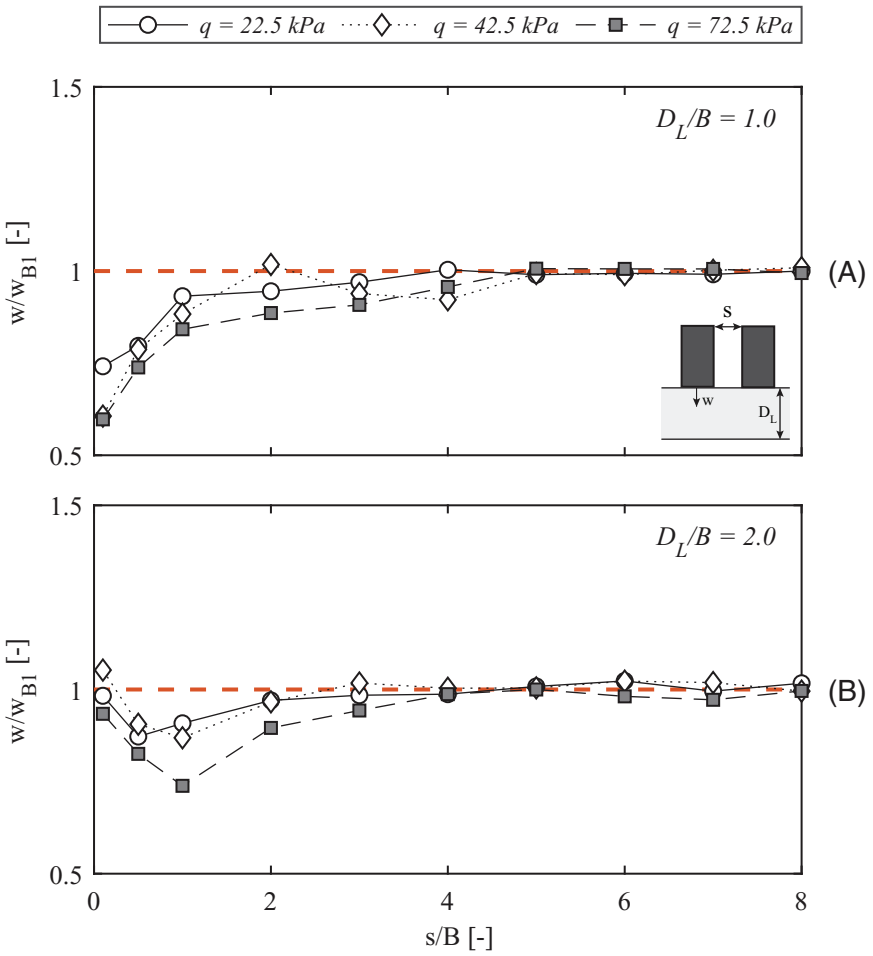

FIGURE 12 The effect of SSSI for pairs of identical neighboring structures. Settlement (w) normalized to that of the corresponding single building (w_{B1}) in function of normalized gap (s/B) between the buildings, for the three examined structures and the two liquefiable layer depths: (A) $D_L/B = 1$; and (B) $D_L/B = 2$

1 and 2), in function of the gap between the structures. The settlement (w) is normalized to the corresponding single, isolated building (w_{B1}), while the gap (s) between the buildings is normalised to the width of building ($B = 5\ m$).

A first key conclusion is the beneficial effect of SSSI on settlements, which are lower than or equal to the settlement of the corresponding single building for all cases examined: $w/w_{B1} \leq 1$. This prediction is consistent with the experimental centrifuge observations of Hayden et al.[29] and Jafarian et al.[30] In the case of the shallow ($D_L/B = 1$) layer (Figure 12A), the decrease of the normalized gap (s/B) leads to a decrease of the normalized settlement (w/w_{B1}). This beneficial effect is attributed to the development of the aforementioned column of stiffer soil underneath the foundations. When the two neighboring structures are close to each other, the developing stiffer soil columns tend to be united, forming a wider column of double the width ($2B$). It is therefore no surprise that the effect of SSSI increases with the bearing pressure, with the settlement of the heavily-loaded ($q = 72.5\ kPa$) buildings not exceeding 60% of that of the corresponding single building. The developing stiffer soil columns become more-and-more independent as the gap between the structures increases, and at $s/B = 2$, the settlement is not affected anymore: $w/w_{B1} \approx 1$.

The effect of SSSI is still beneficial, but less pronounced in the case of the deeper ($D_L/B = 2$) layer (Figure 12B). Interestingly, a different trend is observed. Three areas can be identified in the graph, in function of the gap (s/B) between the buildings. When the buildings are very close to each other ($s/B \leq 0.1$), the settlement is practically equal to that of the single building: $w/w_{B1} \approx 1$. In contrast to the previously discussed shallow layer, the developing stiffer soil bulbs cannot reach the base of the model (see also Figure 8B), and therefore the beneficial support columns cannot form. As a result, the two developing stiffer soil bulbs tend to "float" in the liquefied soil. When they are close to each other, the static shear stresses at the edges of the two foundations are cancelled out, and the two foundations tend to behave as a wider, flexible (hinged in the middle) foundation, consisting of two rigid foundations. This can be better visualized in Figure 13A, where the accumulated shear strain contours are plotted at the end of shaking ($t = 17\ s$). Although the two stiffer soil bulbs intersect, they still cannot reach the layer base.

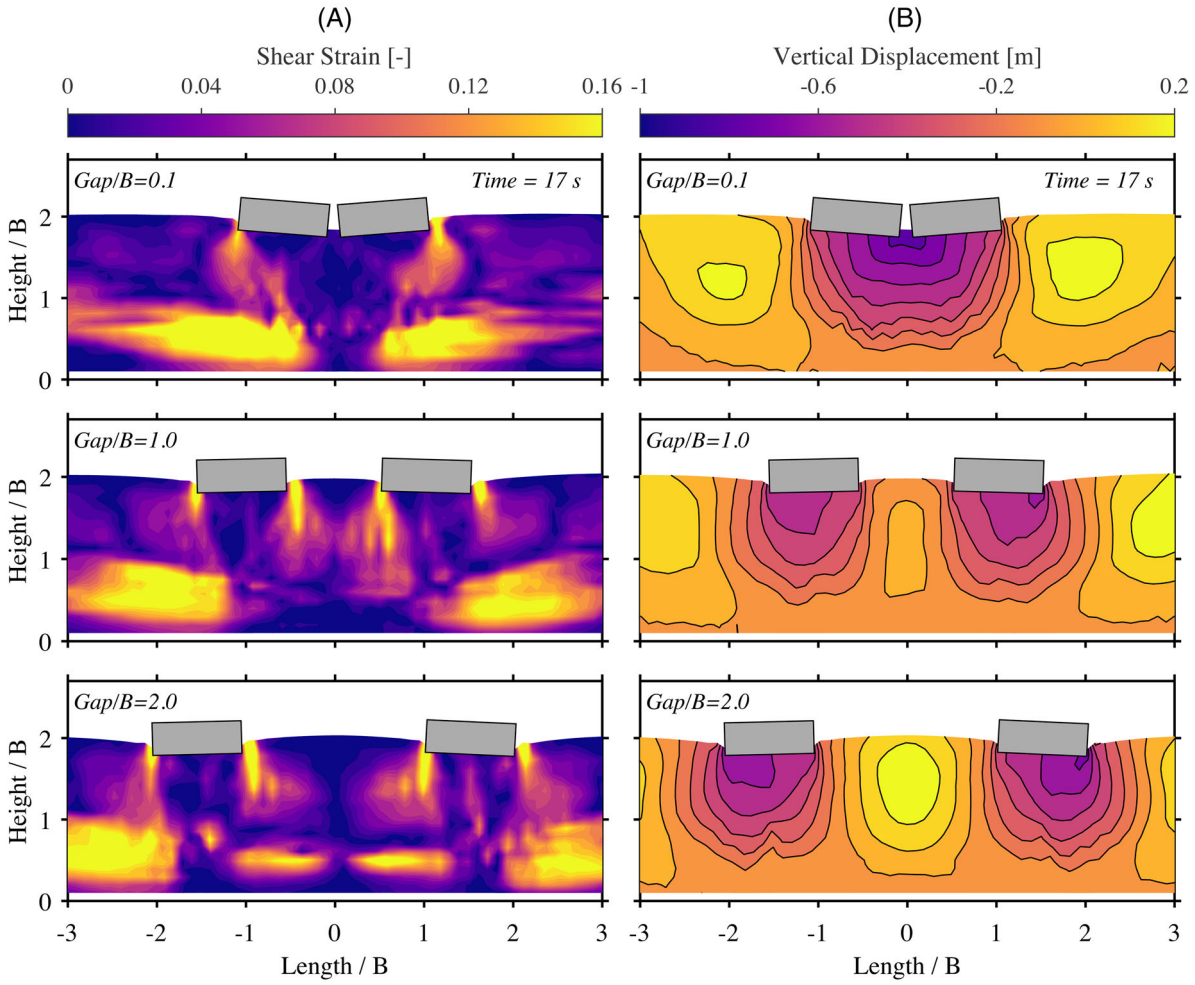

FIGURE 13 The effect of SSSI for pairs of identical neighboring structures on a $D_L/B = 2$ liquefiable layer for $t = 17\ s$. Contours of: (A) accumulated shear strain (γ); and (B) settlement (w) for $s/B = 0.1,\ 1\ and\ 2$

Thereafter, and up to $s/B = 1$, the increase of the gap has a beneficial effect on w. Due to the increased distance between the structures, the static shear stresses at the foundation edges are not cancelled out, and the two foundations behave as two independent foundations. However, the developing failure mechanisms are not independent, intersecting each other. As a result, the soil wedge that develops between the two foundations is not free to uplift (as kinematically required), leading to an increase of bearing capacity, which results to the observed reduction of settlement. This is confirmed by the contours of settlement (w) at the end of shaking (Figure 13B).

Further increase of s/B, leads to progressive separation of the two failure mechanisms, which leads to a decrease of bearing capacity and, consequently, to an increase of settlement. For $s/B = 2$, the two mechanisms are adequately (but not totally) independent (Figure 13), and therefore the normalized settlement w/w_{B1} tends (but is not equal) to 1. A sufficiently larger gap is required to achieve full separation of the two failure mechanisms, which is of the order of $s/B = 5$ (Figure 13).

5.2 | Rotational response

Although SSSI has a beneficial effect on settlement, this is not necessarily the case when examining the residual rotation (ϑ) of the buildings. Figure 14 summarizes the results in terms of ϑ, for all of the studied pairs of buildings and for the shallow and deep liquefiable soil layers. The dotted line denotes the residual rotation of the corresponding single building. As for settlement, a sufficiently large gap between the buildings, of the order of $s/B = 5$, is necessary for the residual rotation to be unaffected by the presence of the neighboring building for both layer depths, $D_L/B = 1$ (Figure 14) and $D_L/B = 2$ (Figure 14). However, for smaller s/B, SSSI leads to quite a significant increase of ϑ for all cases examined,

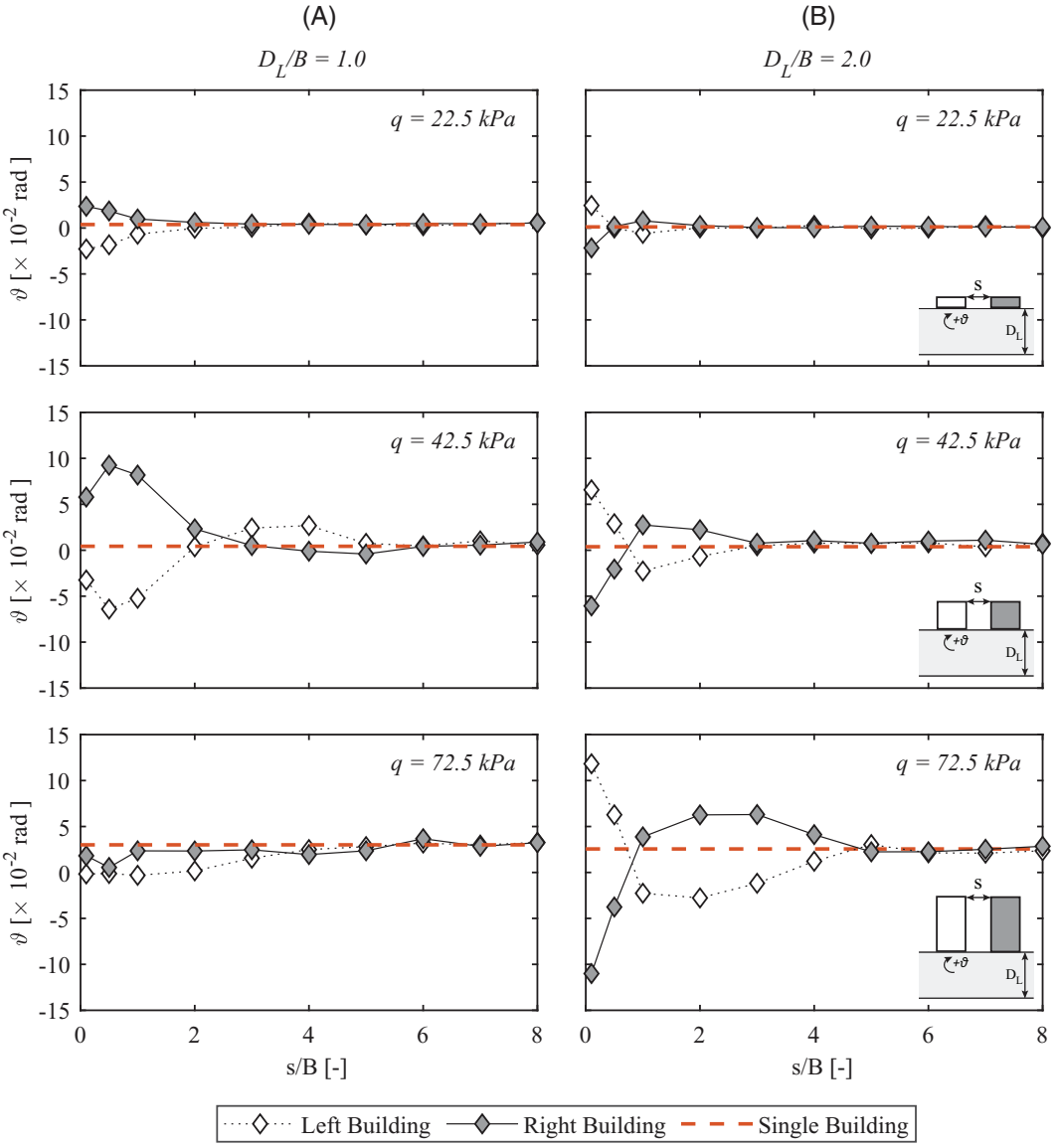

FIGURE 14 The effect of SSSI for pairs of identical neighboring structures. Residual rotation (ϑ) in function of normalized gap (s/B) between the buildings, for the three examined structures and the two liquefiable layer depths: (A) $D_L/B = 1$; and (B) $D_L/B = 2$

with the only exception being the heavily-loaded buildings on the shallow layer. In the case of the lightly-loaded buildings in the deep layer ($D_L/B = 2$), the residual rotation is increased by 2.3×10^{-2} rad leading to a rotation, which is up to 23 times larger than that of the single building. The effect of SSSI on ϑ is reduced with increasing bearing pressure, with its increase being up to 22 and 5 times for the moderately- and the heavily-loaded pairs of buildings, respectively. In cases, ϑ is significantly higher than the ultimate tilt limit of 1/50 (0.02 rad), after which a building is considered dangerous and remedial action or demolition is urgently required[40]. On the contrary, SSSI has a beneficial effect on ϑ for the heavily-loaded buildings on the shallow layer (Figure 14A). This beneficial effect is observed only in this case, which is also the only case where the stiffer soil columns below the foundations reach the base of the layer.

The direction of rotation is another interesting conclusion that arises from Figure 14. For the shallow ($D_L/B = 1$) layer, the two buildings consistently tend to rotate away from each other. A different trend is observed for the deep ($D_L/B = 2$) layer, where the buildings tend to rotate towards each other for $s/B < 1$. Interestingly, with the increase of s/B beyond 1 the two buildings tend to rotate away from each other, as for the shallow layer. These trends are better visualised in Figure 15, where the change in distance $(L - s)/H$ between the top inner corners of the neighboring buildingsm, normalised with the height of each building, is plotted against their normalized gap s/B, for the moderately- and the heavily-loaded buildings.

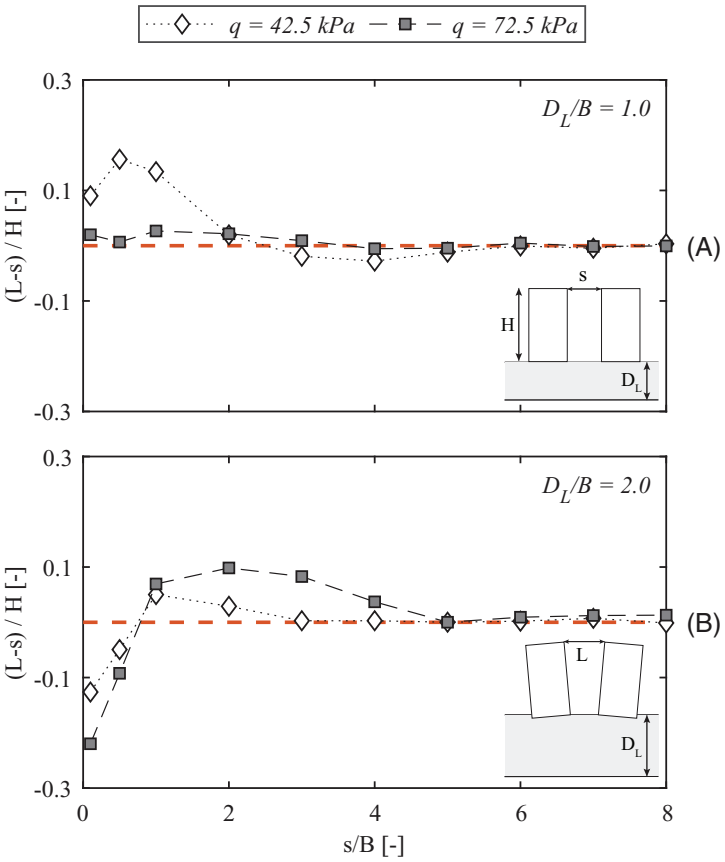

FIGURE 15 Change in distance $(L - s)/H$ between the top inner corners of the buildings (gap opening when positive, closure when negative) in function of initial gap s/B for moderately- and heavily-loaded buildings, and liquefiable layer depth: (A) $D_L/B = 1$; and (B) $D_L/B = 2.3$

Positive values of $(L - s)/H$ correspond to an increase of distance. Potential collision between the two buildings has not been considered, and therefore negative values of of $(L - s)/H$ are possible in these results, even for $s/B = 0$.

In the case of the shallow ($D_L/B = 1$) layer (Figure 15A), both the heavily- and the moderately-loaded buildings tend to rotate away from each other, when $s/B \leq 2$. For larger initial gap s/B, the effect of SSSI is progressively reduced and the response converges to that of a single building. The opening $(L - s)/H$ between the top corners of the buildings is less pronounced for the heavily-loaded buildings, where the developing stiffer soil column reaches the base of the layer (Figure 8), preventing excessive deformations.

The reason why the buildings tend to rotate away from each other for $s/B < 2$ is further elucidated in Figure 16, which depicts the total displacement (u) contours for the moderately-loaded buildings on the shallow layer, for $s/B = 0.1$, 0.5, and 2. Due to the proximity of the rigid base of the soil layer, a deep failure mechanism cannot develop, and a more shallow bearing capacity failure mechanism is mobilised.[41–43] The developing failure mechanism cannot reach the inner foundation corner, due to the shallow depth of the layer, but also due to the increased confinement between the two foundations.

When the two buildings are close to each other, the initial shear stresses at the inner foundation edges tend to cancel out, or at least reduce significantly compared to the ones developing at the outer edges (are demonstrated for the deeper layer in Figure 13). In addition to the reduced shear stress, the soil between the two foundations is also more confined, due to the formation of the stiffer soil column. As a result, shear strains predominantly accumulate at the outer edges of the two foundations, leading to the observed rotation of the building away from each other. The toppling collapse of the Teverler buildings shown in Figure 1B can be classified in this category. In that specific case, the two buildings were located next to each other, and were founded on top of a 2 m thick silt layer (ML), which is believed to have liquefied during the 1999 Kocaeli earthquake.[3]

In the case of the deep ($D_L/B = 2$) layer, the response can be distinguished in three different regions. For $s/B \geq 5$ (Figure 17A), the two buildings are adequately away from each other and the developing failure mechanisms do not interfere with each other. Hence, SSSI does not affect significantly the response, which is similar to that of a single building. For $1 < s/B < 5$ (Figure 17B), a response similar to the one previously described for the shallow layer is observed, with the two buildings tilting away from each other (Figure 15B). Each of the two buildings generates a soil bulb of stiffer soil,

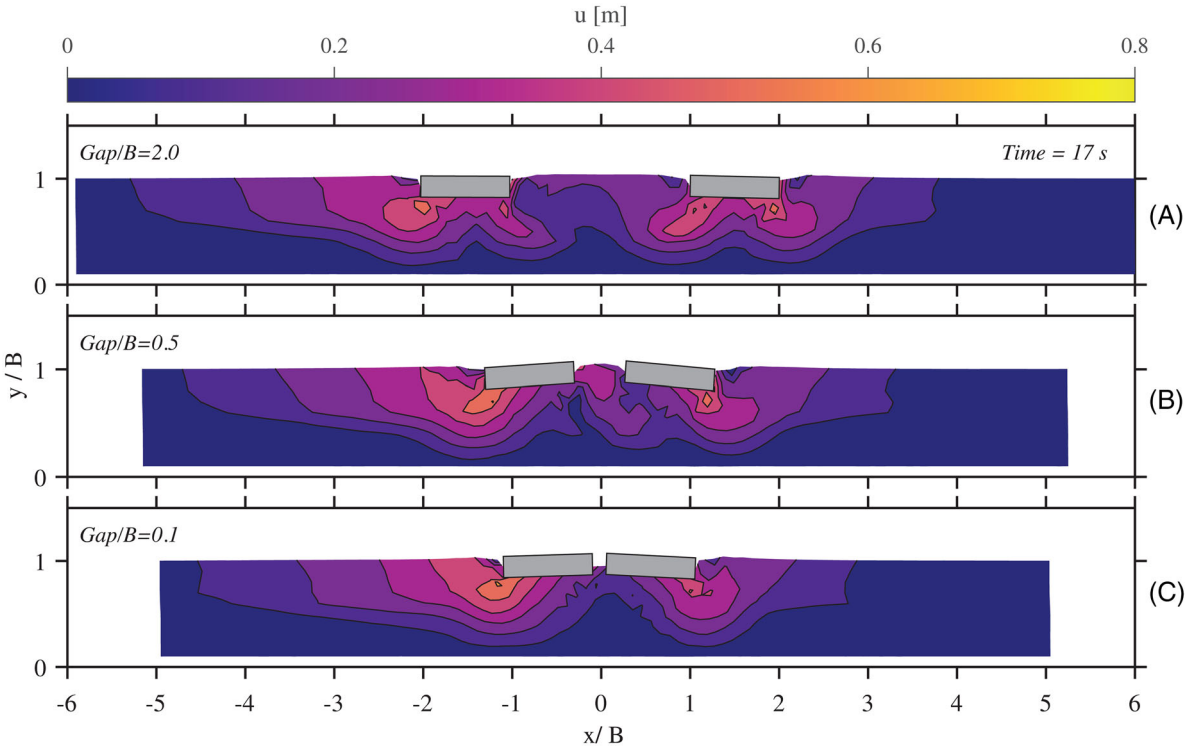

FIGURE 16 Contours of total displacement (u) at the end of shaking ($t = 17\ s$) for $q = 42.5\ kPa$ and liquefiable layer depth $D_L/B = 1$, for: (A) $s/B = 2$; (B) $s/B = 1$; and (C) $s/B = 0.1$

which intersects with the shear mechanism developed by its neighboring structure. Since the two shear zones intersect, the bearing capacity failure mechanism cannot fully develop between the two structures (see also Figure 13A), facilitating accumulation of shear strains on the other side (the outer edges of the two buildings). Moreover, the presence of the neighboring foundation acts as a kinematic constraint, preventing the development of an inner failure wedge (Figure 17B). As a result, the two buildings rotate away from each other.

Interestingly, for $s/B < 1$ the buildings start rotating towards each other. In this case, the two foundations are so close that they can be considered to behave as a single flexible (hinged) foundation of width $2B$. Due to the larger depth of the liquefiable layer, the developing stiffer soil bulbs cannot reach the base of the layer, "floating" in the softened liquefied soil. The failure mechanism observed in Figure 17C is similar with the failure mechanism of a single building (Figure 11B), with the soil in the stiffer soil bulb beneath the two neighboring foundations forming a triangular wedge that moves downwards, displacing the adjacent soil towards the free-field (left and right). Because the maximum vertical displacement is at the centre of the flexible foundation the two structures tilt inwards

6 | CONCLUSIONS

This paper has studied the effect of structure–soil–structure interaction (SSSI) on the seismic response of neighboring structures, founded on shallow strip foundations on liquefiable sand. The problem was studied through coupled hydromechanical analyses, employing the FD code FLAC2d, modelling nonlinear soil response with PM4sand. The model was calibrated against soil element tests of Hostun (HN31) sand with initial void ratio $e = 0.838$, conducted at the ETHZ geotechnical laboratory[18]. The numerical methodology has been compared against 6 centrifuge model tests of different liquefiable layer depths and foundation bearing pressures, where the ability to predict settlements was showcased. For a detailed outline of the strengths and the limitations of the numerical methodology the reader is referred to in Kassas et al.[19]

Three idealized building structures were analyzed, varying the height (and therefore the aspect ratio), the foundation bearing pressure (q), and the depth of the liquefiable layer (D_L/B). Before studying the effect of SSSI on the response of neighboring structures, the corresponding reference cases of single building configurations were analyzed. In the case

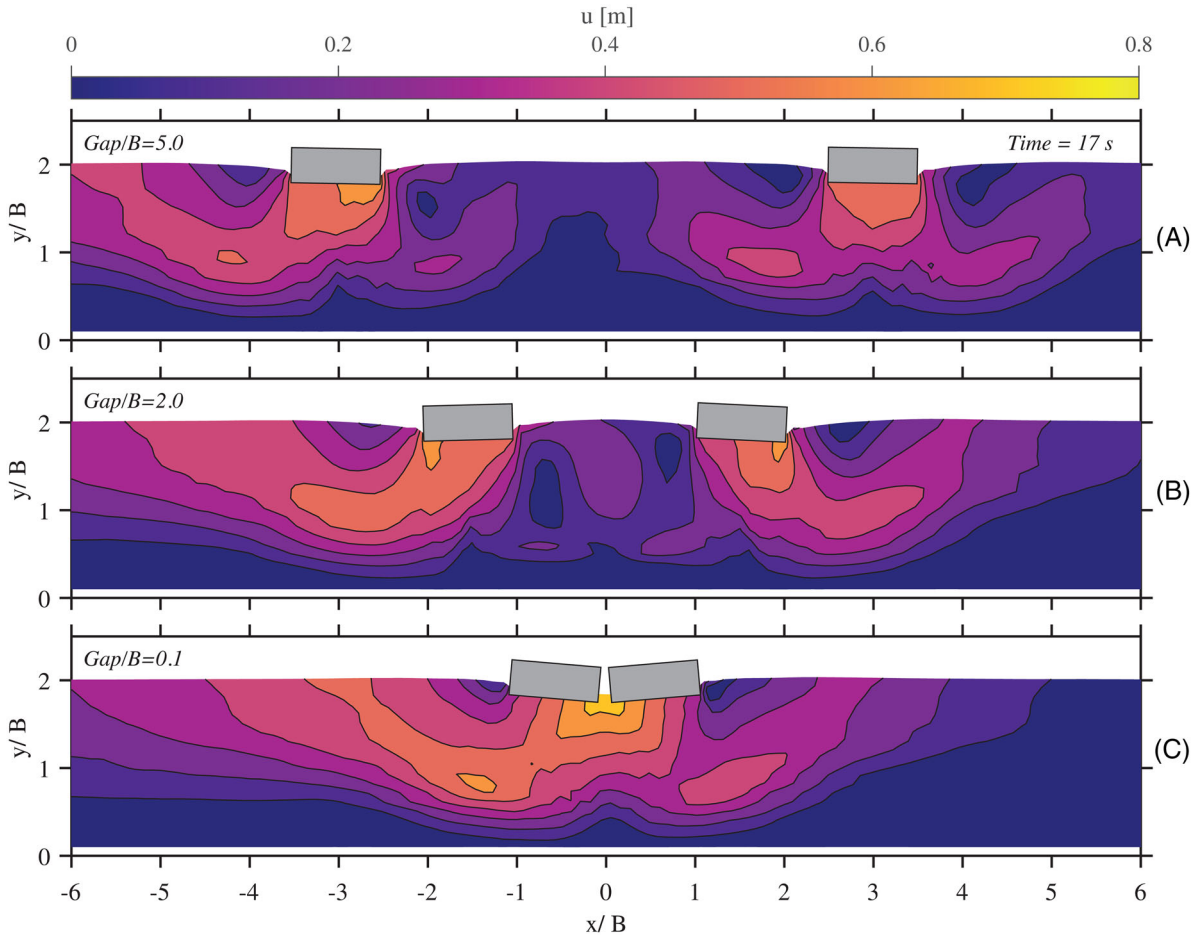

FIGURE 17 Contours of total displacement (u) at the end of shaking ($t = 17\ s$) for $q = 72.5\ kPa$ and liquefiable layer depth $D_L/B = 1$, for: (A) $s/B = 5$; (B) $s/B = 2$; and (C) $s/B = 0.5$

of a deep ($D_L/B = 2$) liquefiable layer, the settlement was found to increase with foundation bearing pressure q, due to the increase of the rocking moments and the developing shear stresses in the soil. In stark contrast, the increase of q was shown to have a beneficial effect on settlement in the case of the more shallow ($D_L/B = 1$) layer. The increase of q was shown to lead to increased confinement, resulting to the development of a stiffer soil column going all the way to the base of the shallow layer, which offers better support to the overlying structure. The presence of the stiffer soil column does not allow redistribution of static shear stresses below the foundation edges, thus preventing shear stress reversals. As a result, the stress path does not pass through the origin, leading to a reduction of the accumulated shear strains, thus reducing the liquefaction-induced foundation settlement.

Pairs of identical structures were subsequently analysed, revealing the effect of SSSI on co-seismic settlement and rotation. The assumption of a single (isolated) building was shown to be an oversimplification, as SSSI can have a significant *beneficial* or *detrimental* effect on performance, altering the response of the structure not only quantitatively but also qualitatively, by leading to the development of fundamentally different deformation mechanisms. More specifically, the numerical predictions, in agreement with experimental centrifuge observations,[29] showed that SSSI has a *beneficial* effect on settlement w, leading to up to a 40% reduction. In stark contrast, its effect on permanent building rotation ϑ was shown to be *detrimental*, leading to its significant increase compared to the equivalent single structure.

The advanced numerical methodology allowed the in-depth assessment of the effects of SSSI through a parametric numerical analysis as a function of the foundation bearing pressure (q), the depth of the liquefiable layer (D_L/B) and the gap (s/B) between the neighboring structures. The detrimental effect of SSSI on ϑ was shown to be a function of the gap (s/B) between neighboring structures, in combination with the liquefiable layer depth (D_L/B). A sufficiently large gap of the order of $s/B = 5$ is required for the residual ϑ not to be affected by the neighboring structure. In the case of the shallow ($D_L/B = 1$) layer, the two buildings were consistently shown to rotate away from each other. When the buildings

are in close proximity, the initial shear stresses under the inner foundation edges tend to cancel out. Combined with the formation of a stiffer soil column, this leads to larger accumulation of shear strains at the outer foundation edges, resulting to their outward rotation. In the case of the deeper ($D_L/B = 2$) layer, for $1 < s/B < 5$, the response is similar, with the two buildings tilting away from each other. However, when the buildings are in close proximity ($s/B < 1$), they tend to rotate towards each other. In this case, the two foundations are so close that they behave as a single flexible (hinged) foundation of width $2B$. The triangular wedge that forms below the foundation has its maximum vertical displacement at its centre and thus the foundations rotating towards each other.

It is worth pointing out that the numerical investigations included in this study focused on homogenous layers of liquefiable sand, using a pseudo-harmonic excitation and buildings that behave as rigid blocks. Additionally, both the depth of the liquefiable layer (D_L/B) and the gap (s/B) between the neighboring structures were parametrically investigated varying D_L and s, while the foundation width (B) remained constant. To that end, the results contained in this paper are meant to be illustrative of the key mechanisms that govern the problem. Quantitatively, the results can change based on the soil profile, building characteristics, and input motion chosen.

ACKNOWLEDGMENT

Open access funding provided by Eidgenossische Technische Hochschule Zurich.

DATA AVAILABILITY STATEMENT

The data that support the findings of this study are available from the corresponding author upon reasonable request.

ORCID

Ioannis Anastasopoulos https://orcid.org/0000-0002-8908-4591

REFERENCES

1. Cubrinovski M, Bradley B, Wotherspoon L, et al. Geotechnical aspects of the 22 February 2011 Christchurch earthquake. *Bull N Z Soc Earthq Eng*. 2011;44(4):205-226.
2. Serikawa Y, Miyajima M, Yoshida M, Matsuno K. Inclination of houses induced by liquefaction in the 2018 Hokkaido Iburi-tobu earthquake, Japan. *Geoenvironmental Disasters*. 2019; 6(1): 1-9.
3. Bray JD, Sancio RB, Durgunoglu T, et al. Subsurface Characterization at Ground Failure Sites in Adapazari, Turkey. *J Geotech Geoenviron Eng*. 2004; 130(7):673-685.
4. Sancio RB, Bray JD, Stewart JP, et al. Correlation between ground failure and soil conditions in Adapazari, Turkey. *Soil Dyn Earthquake Eng*. 2002; 22(9–12): 1093-1102.
5. Gazetas G, Apostolou M, Anastasopoulos I, Seismic Uplifting of Foundations on Soft Soil, with Examples from Adapazari (Izmit 1999, Earthquake), BGA International Conference on Foundations – Innovations, Observations, Design & Practice in the University of Dundee, Scotland, September 2–5. 2003:37–50.
6. Bertalot D, Brennan AJ, Villalobos FA. Influence of bearing pressure on liquefaction-induced settlement of shallow foundations. *Géotechnique*. 2013;63(5):391-399.
7. Dashti S, Bray JD, Pestana JM, Riemer M, Wilson D. Mechanisms of seismically induced settlement of buildings with shallow foundations on liquefiable soil. *J Geotech Geoenviron Eng*. 2010;136(1):151-164.
8. Adamidis O, Madabhushi SG. Deformation mechanisms under shallow foundations on liquefiable layers of varying thickness. *Géotechnique*. 2018; 68(7): 1-13.
9. Bertalot D, Brennan AJ. Influence of initial stress distribution on liquefaction-induced settlement of shallow foundations. *Géotechnique*. 2015;65(5):418-428.
10. Beaty M, Byrne PM. An effective stress model for predicting liquefaction behaviour of sand", In Geotechnical earth-quake engineering and soil dynamics. *Geotechnical Special Publication*. 1998;75(1):766-777.
11. Boulanger RW, Ziotopoulou K. Formulation of a sand plasticity plane-strain model for earthquake engineering applications. *Soil Dyn Earthquake Eng*. 2013;53:254-267.
12. Cubrinovski M, Ishihara K. state concept and modified elastoplasticity for sand modelling. *Soils Found*. 1998;38(4):213-225.
13. Dafalias YF, Manzari MT. Simple plasticity sand model accounting for fabric change effects. *J Eng Mech*. 2004;130(6):622-634.
14. Elgamal A-W, Parra E, Yang Z, Dobry R, Zeghal M. Liquefaction constitutive model. In: Lade PV, Yamamuro JA, Balkema AA, eds. Physics and Mechanics of Soil Liquefaction: Proceedings of the International Workshop, *Baltimore, Md.*. 1999: 269-279. 10–11 Sept. 1998. Edited by.
15. Taborda DMG, Zdravković L, Kontoe S, Potts DM. Computational study on the modification of a bounding surface plasticity model for sands. *Comput Geotech*. 2014;59:145-160.
16. Tasiopoulou P, Gerolymos N. Constitutive modeling of sand: formulation of a new plasticity approach. *Soil Dyn Earthquake Eng*. 2016; 82: 205-221. Elsevier.

17. Tsaparli V, Kontoe S, Taborda DMG, Potts DM. A case study of liquefaction: demonstrating the application of an advanced model and understanding the pitfalls of the simplified procedure. *Geotechnique*. 2020;70(6):538-558.
18. Kassas K, Adamidis O, Gerolymos N, Anastasopoulos I. Numerical modelling of a structure with shallow strip foundation during earthquake-induced liquefaction. *Géotechnique*. 2020. https://doi.org/10.1680/jgeot.19.P.277
19. Kassas K, Adamidis O, Anastasopoulos I. Shallow strip foundations subjected to earthquake-induced soil liquefaction: validation, modelling uncertainties, and boundary effects. *Soil Dyn Earthquake Eng*. 2021.
20. Tasiopoulou P, Chaloulos Y, Gerolymos N, Giannakou A, Chacko J, 3D and 2D simulations of liquefaction induced settlements of shallow foundations using Ta-Ger model. Proceedings of the 7th international conference in earthquake geotechnical engineering, Rome, Italy, 2019:pp. 5241-5248.
21. Karamitros DK, Bouckovalas GD, Chaloulos YK. Insight into the seismic liquefaction performance of shallow foundations. *J Geotech Geoenviron Eng*. 2013; 0000797: 599-607. https://doi.org/10.1061/(ASCE)GT.1943-5606
22. Tokimatsu K, Seed HB. Evaluation of settlements in sands due to earthquake shaking. *J Geotech Geoenviron Eng*. 1987;113(8):861-878.
23. Ishihara K, Yoshimine M. Evaluation of settlements in sand deposits following liquefaction during earthquakes. *Soils Found*. 1992; 1(32): 178-188. http://www.mendeley.com/research/geology-volcanic-history-eruptive-style-yakedake-volcano-group-central-japan/ Available at
24. Bray JD, Macedo J. 6th Ishihara lecture: simplified procedure for estimating liquefaction-induced building settlement. *Soil Dyn Earthquake Eng*. 2017;102(August): 215-231.
25. Bullock Z, Karimi Z, Dashti S, Porter K, Liel AB, Franke KW. A physics-informed semi-empirical probabilistic model for the settlement of shallow-founded structures on liquefiable ground. *Geotechnique*. 2019;69(5):406-419.
26. Bullock Z, Karimi Z, Dashti S, Porter K, Liel AB, Franke KW. A physics-informed semi-empirical probabilistic model for the settlement of shallow-founded structures on liquefiable ground. *Géotechnique*. 2019;69(5):406-419.
27. Adamidis O, Madabhushi SG. Rocking response of structures with shallow foundations on thin liquefiable layers. *Géotechnique*. 2021. https://doi.org/10.1680/jgeot.19.P.077
28. Haigh SK, Madabhushi G. Centrifuge modeling of seismic liquefaction effects on adjacent shallow foundations. *ICPMG*. 2014: 1039-1044.
29. Hayden CP, Zupan JD, Bray JD, Allmond JD, Kutter BL. Centrifuge tests of adjacent mat-supported buildings affected by liquefaction. *J Geotech Geoenviron Eng*. 2015; 141(3): 04014118.
30. Jafarian Y, Mehrzad B, Lee CJ, Haddad AH. Centrifuge modeling of seismic foundation-soil-foundation interaction on liquefiable sand. *Soil Dyn Earthquake Eng*. 2017; 97(March): 184-204.
31. kirkwood p, dashti s. a centrifuge study of seismic structure-soil- structure interaction on liquefiable ground and implications for design in dense urban areas. *Earthquake Spectra Preprint*. 2018. https://doi.org/10.1193/052417EQS095M
32. Qi S, Knappett JA. Effect of soil permeability on soil–structure and structure–soil–structure interaction of low-rise structures. *Géotechnique, (Ca V)*. 2021: 1-16.
33. *Itasca. FLAC – Fast Lagrangian Analysis of Continua, Version 8.0*, Itasca Consulting Group, 2019.
34. Boulanger RW, Ziotopoulou K. A sand plasticity model for earthquake engineering applications. *UCD/CGM-15(May)*. 2017:1-114.
35. Ziotopoulou K, Boulanger RW. Plasticity modeling of liquefaction effects under sloping ground and irregular cyclic loading conditions. *Soil Dyn Earthquake Eng*. 2016;84:269-283. Elsevier.
36. Aldaikh H, Alexander NA, Ibraim E, Knappett J. Shake table testing of the dynamic interaction between two and three adjacent buildings (SSSI)". *Soil Dyn Earthquake Eng*. 2016;89:219-232.
37. Mason H, Trombetta N, Chen Z, Bray J, Hutchinson T, Kutter B. Seismic soil–foundation–structure interaction observed in geotechnical centrifuge experiments. *Soil Dyn Earthquake Eng*. 2013; 48: 162-174.
38. Trombetta NW, Mason HB, Chen Z, Hutchinson TC, Bray JD, Kutter BL. Nonlinear dynamic foundation and frame structure response observed in geotechnical centrifuge experiments. *Soil Dyn Earthquake Eng*. 2013; 50: 117-133.
39. Trombetta NW, Mason HB, Hutchinson TC, Zupan JD, Bray JD, Kutter BL. Nonlinear soil – foundation – structure and structure – soil – structure interaction: engineering demands. *ASCE J Struct Eng*. 2014;141(7):1-12.
40. Charles JA, Skinner HD. Settlement and tilt of low-rise buildings. *Proc Inst Civ Eng Geotech Eng*. 2004;157(2):65-75.
41. Lundgren H, Mortensen K, Determination by the theory of plasticity of the bearing capacity of continuous footing on sand, Proceedings Third International Conference on Soil Mechanics and Foundation Engineering. Zurich, Switzerland. 1953: 409-412.
42. Mandel J, Salencon J, 'Force portante d ' un sol sur une assise rigide (Ctude thkorique). 1972;(1):79-93.
43. Sethy BP, Patra CR, Das BM, Sobhan K. Behavior of circular foundation on sand layer of limited thickness subjected to eccentrically inclined load. *Soils and Foundations*. 2020; 60(1): 13-27. Japanese Geotechnical Society.

How to cite this article: Kassas K, Adamidis O, Anastasopoulos I. Structure–soil–structure interaction (SSSI) of adjacent buildings with shallow foundations on liquefiable soil. *Earthquake Engng Struct Dyn*. 2022;51:2315-2334. https://doi.org/10.1002/eqe.3665